

Pinwheel stability, pattern selection and the geometry of visual space

Michael Schnabel^{1,2}, Matthias Kaschube^{1,2,3,4} and Fred Wolf^{1,2}

¹Max Planck Institute for Dynamics and Self-Organization, Goettingen, Germany, ²Bernstein Center for Computational Neuroscience, University of Goettingen, Goettingen, Germany, ³Lewis-Sigler Institute,

⁴Physics Department, Princeton University, Princeton, New Jersey, USA

It has been proposed that the dynamical stability of topological defects in the visual cortex reflects the Euclidean symmetry of the visual world. We analyze defect stability and pattern selection in a generalized Swift-Hohenberg model of visual cortical development symmetric under the Euclidean group $E(2)$. Euclidean symmetry strongly influences the geometry and multistability of model solutions but does not directly impact on defect stability.

When an object in the visual world is rotated about the axis of sight the orientations of distant contours change in a coordinated manner, leaving relative orientations of distant contours invariant. In the visual cortex of the brain, it has been predicted that this geometrical property of visual space imposes the so called shift-twist symmetry on joint representations of contour position and contour orientation [1]. This symmetry requires the equivariance of dynamical models for these representations under the Euclidean group $E(2)$. In particular, it has been hypothesized that shift-twist symmetry stabilizes topological pinwheel-defects in models for the emergence of orientation selectivity during cortical development [2, 3, 4]. Pinwheel defects are singular points in the visual cortex around which each orientation is represented exactly once [5, 6, 7]. They are initially generated in the visual cortex at the time of eye opening [8, 9]. This process has been theoretically explained by spontaneous symmetry breaking [10, 11]. Why in the brain, pinwheels remain present at all developmental stages, although they are dynamically unstable in many models of visual cortical development [2, 3, 11, 12, 13, 14] and in analogous physical systems [15, 16, 17], remains unclear.

Previous studies [2, 3, 11, 12, 13, 14] found pinwheels dynamically unstable only in models exhibiting an $E(2) \times U(1)$ symmetry, which is higher than the $E(2)$ symmetry of visual perceptual space. In contradistinction, models exhibiting only Euclidean symmetry have been shown to exhibit stable pinwheels [2, 3, 18] suggesting that the stabilization of pinwheel defects may be closely related to the 'reduced' Euclidean symmetry. There are, however, also other scenarios that predict the emergence of stable pinwheels with higher than Euclidean symmetry [12, 14] leaving it hard to judge to actual role of Euclidean symmetry in orientation map development.

Here we analyze the impact of Euclidean symmetry on pattern selection, i.e. the question of whether stable pinwheel arrangement exist and what their geometric organization is. We construct a generalized Swift-Hohenberg model [19, 20] symmetric under the Euclidean group $E(2)$ that allows to study the transition from higher $E(2) \times U(1)$ to lower $E(2)$ symmetry by changing a parameter that controls the strength of shift symmetry breaking (SSB). Using weakly nonlinear analysis we derive ampli-

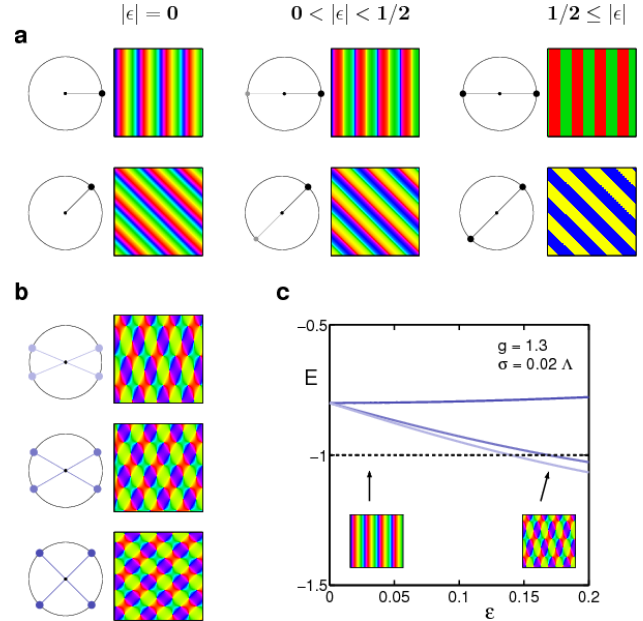


Figure 1: (a) Plane waves with wavevector in horizontal (top) and oblique (bottom) direction for variable strength of SSB ($\epsilon = 0, 0.35, 1$) (b) PWCs of varying intersection angle α , $\pi/4 \leq \alpha \leq \pi/2$. (c) Energy of solutions depends on ϵ and on α . For sufficiently large ϵ PWCs are energetically favored relative to plane waves. (dashed: energy of plane waves, plain: energies of PWCs for $\alpha = \pi/4, \pi/3, \pi/2$)

tude equations for stationary planforms and find three classes of stationary solutions: stripe patterns without any pinwheels, pinwheel crystals with pinwheels regularly arranged on a rhombic lattice, and quasi-periodic patterns containing a large number of irregularly spaced pinwheels. We calculate the phase diagram of these solutions depending on the strength of SSB, the effective strength of nonlocal interactions, and the range of nonlocal interactions. With increasing strength of SSB, pinwheel free patterns are progressively replaced by pinwheel crystals in the phase diagram while both pinwheel free patterns and pinwheel crystals remain stable. Phases of aperiodic pinwheel rich patterns remain basically unaffected. A critical strength of SSB exists above which multistable aperiodic patterns collapse into a single aperiodic state.

The spatial structure of an OPM can be represented by a complex field $z(\mathbf{x})$ where \mathbf{x} denotes the 2D position of neurons in the visual cortex, $\theta(\mathbf{x}) = \arg(z(\mathbf{x}))/2$ their preferred stimulus orientation, and the modulus $|z(\mathbf{x})|$ is a measure of their selectivity [10]. In this representation, pinwheel centers are zeros of the field $z(\mathbf{x})$. The simplest models for the formation of OPMs are defined by a dynamics

$$\partial_t z(\mathbf{x}, t) = F[z](\mathbf{x}, t). \quad (1)$$

where t denotes time and $F[z]$ is a nonlinear operator. We assume the dynamics equivariant under translation $T_{\mathbf{y}}z(\mathbf{x}) = z(\mathbf{x} + \mathbf{y})$, rotation $R_{\alpha}z(\mathbf{x}) = e^{2i\alpha}z(\Omega_{-\alpha}\mathbf{x})$ with rotation matrix Ω_{ϕ} , and reflection at the cortical (1,0) axis $Pz(\mathbf{x}) = \bar{z}(\bar{\mathbf{x}})$, thus expressing the fact that within cortical layers there are no special locations or directions [21]. In addition, if interactions between OPM development and visuotopy are neglected it is also equivariant under global shifts of orientation preference $S_{\beta}z(\mathbf{x}) = e^{i\beta}z(\mathbf{x})$ (*shift symmetry*). Rotations R thus consist of a composition of phase shifts S and coordinate rotations D , i.e. $R_{\alpha} = S_{2\alpha} \circ D_{\alpha}$ with $D_{\alpha}z(\mathbf{x}) = z(\Omega_{-\alpha}\mathbf{x})$.

We consider the general class of variational models [3, 10, 14] for which $F[z]$ has the form

$$F[z] = Lz + \epsilon M\bar{z} + N_3[z]. \quad (2)$$

Here L is a linear, translation invariant and self-adjoint operator, that accounts for a finite wavelength instability. N_3 is a cubic nonlinearity which stabilizes the dynamics. The second term involves a complex conjugation $Cz = \bar{z}$ and thus manifestly breaks shift symmetry when $\epsilon \neq 0$. M is assumed to be linear, translation invariant and bounded. Equivariance under rotations, $[MC, R_{\alpha}] = 0$, requires

$$D_{\alpha}MD_{\alpha}^{-1} = S_{-4\alpha}M \quad (3)$$

and equivariance under parity $[M, P] = 0$.

As a concrete example we will consider the model

$$L = r - (k_c^2 + \nabla^2)^2 \quad (4)$$

$$N_3[z] = (1 - g)|z(\mathbf{x})|^2 z(\mathbf{x}) - \frac{2 - g}{2\pi\sigma^2} \quad (5)$$

$$\times \int d^2y \left(|z(\mathbf{y})|^2 z(\mathbf{x}) + \frac{1}{2} z(\mathbf{y})^2 \bar{z}(\mathbf{x}) \right) e^{-|\mathbf{y}-\mathbf{x}|^2/2\sigma^2}$$

$$M = r(\partial_x + i\partial_y)^4 (\partial_{xx} + \partial_{yy})^{-2} \quad (6)$$

where L is the Swift-Hohenberg operator [19, 20] with critical wavenumber k_c and instability parameter r . N_3 is adopted from [14], where σ sets the range of the nonlocal interactions and g determines whether the local ($g > 1$) or the nonlocal term ($g < 1$) stabilizes the dynamics. M is the simplest differential operator which transforms according to Eq.(3). It is unitary with spectrum $\propto e^{4i \arg(\mathbf{k})}$.

We used weakly nonlinear analysis [22] to study potential solutions of Eq.(2). We consider planforms $z(\mathbf{x}) =$

$\sum_{j=0}^{2n-1} A_j e^{i\mathbf{k}_j \mathbf{x}}$, $\mathbf{k}_j = k_c(\cos \alpha_j, \sin \alpha_j)$ with $2n$ modes where we require that to each mode also its antiparallel mode is in the set. By symmetry, the dynamics of the amplitudes A_j at threshold has the form

$$\dot{A}_j = A_j + \epsilon \bar{A}_{j-} e^{4i\alpha_j} - \sum_{k=0}^{2n-1} g_{jk} |A_k|^2 A_j - \sum_{k=0}^{2n-1} f_{jk} A_k A_{k-} \bar{A}_{j-} \quad (7)$$

where j^- denotes the index of the mode antiparallel to mode j , $\mathbf{k}_{j-} = -\mathbf{k}_j$ and with real valued and symmetric matrices g_{jk} and f_{jk} which determine the coupling and competition between modes. They can be expressed in terms of angle-dependent interaction functions $g(\alpha)$ and $f(\alpha)$, which are obtained from the nonlinearity $N_3[z]$ (cf.[14, 19, 22]). For simplicity we restrict the following analysis to the class of permutation symmetric models, defined in [14], for which $g(\alpha) = g(\alpha + \pi)$. [23]

The simplest solution to Eq.(7) is obtained for $n = 1$ and consists of plane waves with wavevector $\mathbf{k} = k_c(\cos \alpha, \sin \alpha)$. For $|\epsilon| \leq 1/2$ it is given by

$$z(\mathbf{x}) = \frac{e^{2i\alpha}}{\sqrt{g_{00}}} [\sqrt{1 + 2\epsilon} \cos(\mathbf{k}\mathbf{x} + \phi) + i\sqrt{1 - 2\epsilon} \sin(\mathbf{k}\mathbf{x} + \phi)] \quad (8)$$

with arbitrary phase ϕ . Hence with SSB orientation angles are no longer equally represented. For $\epsilon > 0$ cortical area for orientations α and $\alpha + \pi/2$ is recruited at the expense of $\alpha + \pi/4$ and $\alpha + 3\pi/4$ (and vice versa for $\epsilon < 0$). Beyond a critical strength of SSB, $\epsilon_* = 1/2$, patterns only contain two orientations, $z(\mathbf{x}) = e^{2i\alpha} \mathcal{N} \cos(\mathbf{k}\mathbf{x} + \phi)$ for $\epsilon > \epsilon_*$ and $z(\mathbf{x}) = ie^{2i\alpha} \mathcal{N} \sin(\mathbf{k}\mathbf{x} + \phi)$ for $\epsilon < -\epsilon_*$ with $\mathcal{N} = \sqrt{4(1 + |\epsilon|)/3g_{00}}$ (Fig.1a).

Another class of solutions, rhombic pinwheel crystals (PWCs), exist for $n = 2$ and consist of two pairs of antiparallel modes forming an angle $0 < \alpha \leq \pi/2$ which are characterized by $|A_0| = |A_{0-}| = a = |A_1| = |A_{1-}|$. We consider w.l.o.g. the case $\alpha_0 = -\alpha/2$ and $\alpha_1 = \alpha/2$ (Fig.1b). With $A_{0,1} = ae^{i\mu_{0,1}}$, $A_{0-,1-} = ae^{i\nu_{0,1}}$ and $\Sigma_{0,1} := \mu_{0,1} + \nu_{0,1}$ the stationary state is given by $\Sigma_1 = -\Sigma_0$ and $a^2 = (1 + \epsilon \cos(\Sigma_0 + 2\alpha))/\zeta$ where $\zeta = 3g_{00} + 2g_{01} + 2f_{01} \cos 2\Sigma_0$. The phase Σ_0 is the solution to $0 = \sin 2\Sigma_0 + \epsilon[\sin(\Sigma_0 - 2\alpha) - (2 + 3g_{00}/g_{01}) \sin(\Sigma_0 + 2\alpha)]$ which bifurcates from $\Sigma_0 = \pm\pi/2$ for $\epsilon = 0$. The energy is given by $E_{PWC} = -4a^2(1 + |\epsilon| \cos(\Sigma_0 + 2\alpha)) + 2a^4\zeta$. For the model Eqs.(4-6) the ϵ and α dependence of the energy is shown in Fig.1c. The solution then reads $z(\mathbf{x}) = 2a[e^{i\Sigma_0/2} \cos(\mathbf{k}_0\mathbf{x} + \Delta_0/2) + e^{-i\Sigma_0/2} \sin(\mathbf{k}_1\mathbf{x} + \Delta_1/2)]$ with arbitrary Δ_0 and Δ_1 .

A large set of quasiperiodic solutions originates from the essentially complex planforms (ECP) $z(\mathbf{x}) = \sum_{j=0}^{n-1} A_j^+ e^{il_j \mathbf{k}_j \mathbf{x}}$ that solve Eq. (7) for $\epsilon = 0$ [14]. Here, wave vectors $\mathbf{k}_j = k_c(\cos \frac{\pi}{N} j, \sin \frac{\pi}{N} j)$ ($j = 0, \dots, n-1$) are distributed equidistantly on the upper half of the critical circle and binary variables $l_j = \pm 1$ determine whether the mode with wave vector \mathbf{k}_j or with wave vector $-\mathbf{k}_j$ is active (Fig.2(a) *left column*).

For $|\epsilon| > 0$ we find that ECPs generalize to $z(\mathbf{x}) = \sum_{j=0}^{n-1} [A_j^+ e^{il_j \mathbf{k}_j \mathbf{x}} + A_j^- e^{-il_j \mathbf{k}_j \mathbf{x}}]$. For each n there exists

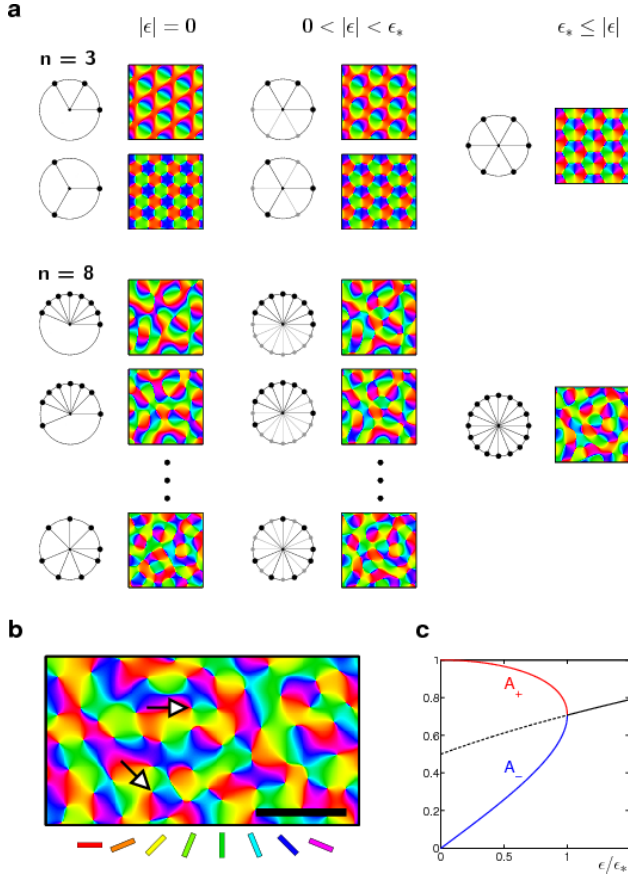


Figure 2: Attractors of amplitude equations (Eq.7) with full, partially broken and completely broken shift symmetry. (a) ECPs. Preferred orientations are color coded [see bars in (b)]. Arrangement of active modes on the critical circle and corresponding OPMs. For $n = 3$ and 8 there are 2 and 15 different classes of ECPs, respectively. Complete (partial, no) suppression of opposite modes for full (weakly broken, maximally broken) shift symmetry (*left, middle, right column*). (b) OPM in tree shrew V1 (data: L.E.White, Duke Univ., USA). Arrows pinwheel centers. Scale bar 1 mm. (c) With increasing degree of symmetry breaking ϵ amplitudes of antiparallel modes A_- grow and eventually (at $\epsilon = \epsilon_*$) reach the same absolute value as active modes A_+ .

a critical value $\epsilon_* := \gamma[g_{00} + 2 \sum_{j=0}^{n-1} f_{ij} \cos \frac{4\pi}{n} j]$, where $\gamma = [2 \sum_{j=0}^{n-1} g_{ij}]^{-1}$. When $|\epsilon| \leq |\epsilon_*|$ stationary amplitudes $a^\pm = |A_j^\pm|$ fulfill $a_\pm^2 = \gamma(1 \pm \sqrt{1 - \epsilon^2/\epsilon_*^2})$. When $|\epsilon| \geq |\epsilon_*|$ the amplitude of antiparallel and active modes are equal $a_\pm^2 = \gamma[1 + |\epsilon|]/[1 + \epsilon_*]$ (Fig.2c). A simple measure of the degree to which SSB affect n -ECPs is

$$q := \frac{\sum_j A_j^+ A_j^- e^{-i \frac{4\pi}{n} j} + c.c.}{\sum_j |A_j^+|^2 + |A_j^-|^2}.$$

For a stationary n -ECP we find $q = \epsilon/|\epsilon_*|$ if $|\epsilon| \leq |\epsilon_*|$ and $q = \text{sign}(\epsilon)$ if $|\epsilon| > |\epsilon_*|$.

Stationary phases $\phi_j^\pm = \arg A_j^\pm$ fulfill the condition $\phi_j^+ + \phi_j^- = (4\pi/n)j$ if $\epsilon > 0$ and $\phi_j^+ + \phi_j^- = (4\pi/n)j + \pi$

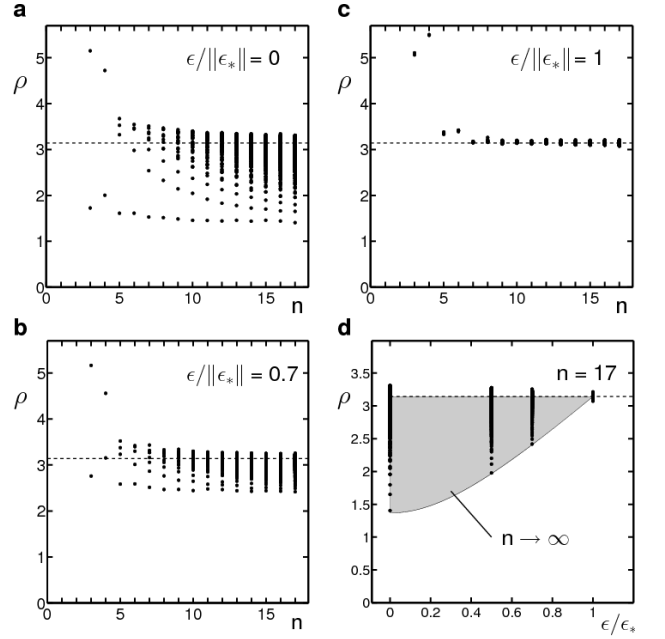


Figure 3: (a)-(c) Pinwheel densities for all realizations of ECPs with $3 \leq n \leq 17$ and different degrees of shift symmetry breaking ϵ . (d) Pinwheel densities for $n = 17$ (dots) and for $n \rightarrow \infty$ in the Gaussian approximation (gray region).

if $\epsilon < 0$. This implies that all orientations are represented in patterns with $n \geq 3$. The solution can be written

$$z(\mathbf{x}) = \sqrt{2\gamma} \sum_{j=0}^{n-1} [\sqrt{1+q} z_j^e(\mathbf{x}, \phi_j) + \sqrt{1-q} z_j^o(\mathbf{x}, \phi_j)]$$

with $z_j^e(\mathbf{x}, \phi_j) = e^{i \frac{2\pi}{n} j} \cos(l_j \mathbf{k}_j \mathbf{x} + \phi_j)$ and $z_j^o(\mathbf{x}, \phi_j) = ie^{i \frac{2\pi}{n} j} \sin(l_j \mathbf{k}_j \mathbf{x} + \phi_j)$ and arbitrary phases ϕ_j . For $n = 1$ this is in agreement with Eq.(8) where $\epsilon_* = 1/2$. Reflection at the axis parallel to \mathbf{k}_j acts on the functions z_j^e and z_j^o as $+1$ and -1 , respectively. Thus z_j^e and z_j^o correspond to the even and odd eigenvectors of the nullspace of $L + \epsilon MC$ (cf.[18]). For $\epsilon > 0$ ($\epsilon < 0$) the even (odd) part dominates the solution.

The dynamics Eq.(7) exhibits a potentially exceedingly high number of multistable solutions. The energy of n -ECPs is given by $E_n = -n\gamma[1 + \epsilon^2/\epsilon_*^2]$ for $|\epsilon| \leq \epsilon_*$ and $E_n = -n\gamma(1 + |\epsilon|)^2/[1 + \epsilon_*]$ for $|\epsilon| \geq \epsilon_*$, respectively, and does not depend on the variables l_j which identify a particular n -ECP. Due to the growth of antiparallel modes with increasing $|\epsilon|$ patterns for all different realizations l_j with phases $\phi_j := l_j \Phi_j + \frac{1}{4}(1 - \text{sign}(\epsilon))(1 - l_j)\pi$ (Φ_j arbitrary but fixed) eventually collapse in a single state $z(\mathbf{x}) \propto \sum_{j=0}^{n-1} z_j^{e/o}(\mathbf{x}, \phi_j)$ (Fig.2a).

This collapse manifests itself in the pinwheel densities ρ_n of various ECPs shown in Fig.3a-c for different strength of SSB. The pinwheel density of an n -ECP in the large n limit is $\rho(\chi) = \pi \sqrt{1 - \frac{8}{\pi^2} (1 - \epsilon^2/\epsilon_*^2) \zeta^2}$ and depends through $\zeta = \frac{1}{4n} |\sum_{j=0}^{n-1} l_j \mathbf{k}_j| \leq 1$ on the configuration of active modes. Fig.3d shows that pinwheel

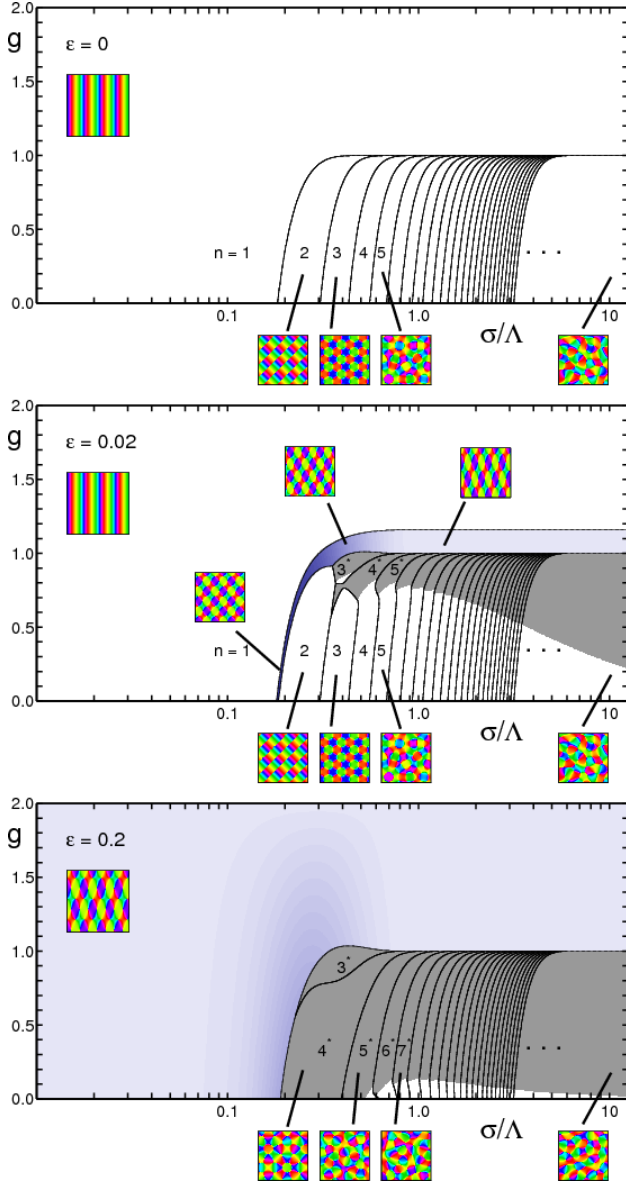


Figure 4: Phase diagrams of the model, Eqs.(4-6), near criticality for variable SSB ϵ . The graph shows the regions of the $g - \sigma/\Lambda$ plane in which n -ECPs and PWCs have minimal energy ($n = 1 - 25$, $n > 25$ dots). Regions of maximally broken shift symmetry [$\epsilon \geq \epsilon_*(N, g, \sigma)$] shaded in *gray*. Regions where α -PWCs prevail is shaded in *blue*, intensity level codes for the relative angle α . (*light blue*: $\pi/4 \leq \alpha \leq \pi/2$:*dark blue*)

densities fill a band of values. With increasing degree of SSB this band narrows and pinwheel densities eventually equal π at the critical value $|\epsilon| = \epsilon_*$.

To reveal how SSB affects pattern selection we calculated the phase diagram for the model specified in Eqs.(4-6) for various values of ϵ . Fig.4 shows the configurations of n -ECPs and PWCs minimizing the energy [24]. Plane waves are progressively replaced by α -PWCs with increasing SSB. Depending on the location in parameter

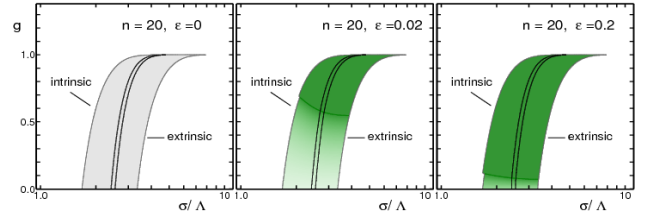


Figure 5: Stability regions of ECPs with $n = 20$ for different ϵ . Dashed line denotes the critical line $\epsilon = \epsilon_*(N, g, \sigma)$, above which $q = 1$. Shaded region denotes region in the $g - \sigma/\Lambda$ plane for which that planform is a stable solution of the dynamics and coexists with planforms of nearby values of n , e.g. $n = 18, 19, 21, 22$. In the inner region (marked by the two inner lines) this solution minimizes energy.

space and on ϵ , a particular angle α minimizing the energy (c.f. Fig.1c). Large n -ECPs are selected when the dynamics is stabilized by long-range interactions ($g < 1$, $\sigma > \Lambda$). In this parameter regime plane waves and pinwheel crystals are unstable. The degree of SSB q manifest in a given n -ECP attractor depends on ϵ and on the location in the phase diagram. Above a critical line defined by $|\epsilon_*(N, g, \sigma)| = |\epsilon|$ antiparallel modes are maximal and $|q| = 1$ (*gray area*), below that line $|q| \leq 1$. Figs. 4 and 5 show the high sensitivity of the dynamics to even small amounts of SSB, a substantial area in phase is occupied by ECPs with $|q| = 1$ even for $\epsilon = 0.02$.

Our analysis of pattern selection in visual cortical development demonstrates that dynamical models of orientation map development are very sensitive to the presence of interactions imposed by Euclidean E(2) symmetry. It also reveals that the impact of the Euclidean symmetry of perceptual visual space is not an all or none phenomenon. For weak SSB our Euclidean model closely mimics the behavior of models possessing the higher E(2)xU(1) symmetry. The only qualitative change that we found in the transition from higher to lower symmetry was the collapse of multistable solutions. This collapse, however, only happens when a finite critical strength of SSB is reached. Up to this threshold strength, models exhibiting E(2) and E(2)xU(1) symmetry seem to be topologically conjugate to one another.

Our analysis also reveals that the impact of Euclidean symmetry differs qualitatively for aperiodic and periodic patterns. For aperiodic patterns, (i) the parameter regime in which they possess minimal energy is virtually unaffected by the strength of SSB, (ii) sets of different multistable solutions become progressively more similar and finally merge forming a single unique ground state, and (iii) Euclidean symmetry geometrically manifests itself in specific two point correlations that are absent in the E(2)xU(1) symmetric limit. For periodic patterns such as pinwheel crystals and pinwheel free states, (i) the parameter regime in which these solutions possess minimal energy depends on the strength of SSB, and (ii) Euclidean symmetry geometrically manifests itself in a specifically selected tilt angle of rhombic pinwheel crys-

tals and a wave vector dependent underrepresentation of particular orientations for pinwheel free states.

The Swift-Hohenberg model of Euclidean symmetry considered here predicts that aperiodic pinwheel rich patterns resembling the architecture of the primary visual cortex are only stable when long-range interactions dominate pattern selection, confirming previous predictions

of a model of higher $E(2) \times U(1)$ symmetry. Our analysis predicts that in this regime, two point correlations provide a sensitive measure of the strength of SSB. Such correlations are therefore a promising tool for probing the impact of Euclidean symmetry in visual cortex development.

-
- [1] P. C. Bressloff, J. D. Cowan, M. Golubitsky, P. J. Thomas, and M. C. Wiener, *Philos Trans R Soc Lond B Biol Sci* **356**, 299 (2001).
 - [2] N. Mayer, J. M. Herrmann, and T. Geisel, *Neurocomputing* **44-46**, 533 (2002).
 - [3] H. Y. Lee, M. Yahyanejad, and M. Kardar, *Proc. Natl. Acad. Sci. U. S. A.* **100**, 16036 (2003).
 - [4] P. C. Bressloff, *Biol Cybern* **93**, 256 (2005).
 - [5] N. V. Swindale, J. A. Matsubara, and M. S. Cynader, *J Neurosci* **7**, 1414 (1987).
 - [6] T. Bonhoeffer and A. Grinvald, *Nature* **353**, 429 (1991).
 - [7] K. Ohki, S. Chung, P. Kara, M. Hubener, T. Bonhoeffer, and R. C. Reid, *Nature* **442**, 925 (2006).
 - [8] L. E. White, D. M. Coppola, and D. Fitzpatrick, *Nature* **411**, 1049 (2001).
 - [9] B. Chapman, M. P. Stryker, and T. Bonhoeffer, *J Neurosci* **16**, 6443 (1996).
 - [10] N. V. Swindale, *Proc R Soc Lond B Biol Sci* **215**, 211 (1982).
 - [11] F. Wolf and T. Geisel, *Nature* **395**, 73 (1998).
 - [12] A. A. Koulakov and D. B. Chklovskii, *Neuron* **29**, 519 (2001).
 - [13] M. W. Cho and S. Kim, *Phys. Rev. Lett.* **92**, 018101 (2004).
 - [14] F. Wolf, *Phys. Rev. Lett.* **95**, 208701 (2005).
 - [15] M.C.Cross and P. Hohenberg, *Rev. Mod. Phys.* **65**, 851 (1993).
 - [16] A. Vilenkin and E. Shellard, *Cosmic Strings and Other Topological Defects* (Cambridge University Press, Cambridge (UK), 1994).
 - [17] E. Bodenschatz, W. Pesch, and G. Ahlers, *Annual Review of Fluid Mechanics* **32**, 709 (2000).
 - [18] P. J. Thomas and J. D. Cowan, *Phys. Rev. Lett.* **92**, 188101 (2004).
 - [19] M. C. Cross and P. C. Hohenberg, *Rev. Mod. Phys.* **65**, 851 (1993).
 - [20] J. Swift and P. C. Hohenberg, *Phys. Rev. A* **15**, 319 (1977).
 - [21] V. Braitenberg and A. Schüz, *Cortex: statistics and geometry of neuronal connectivity* (Springer, Berlin, 1998).
 - [22] P. Manneville, *Dissipative Structures and Weak Turbulence* (Academic Press, San Diego, CA, 1990).
 - [23] For the nonlinearity Eq.(5) one obtains $g(\alpha) = g + (2 - g)e(\alpha)$ and $f(\alpha) = \frac{1}{2}g(\alpha)$ with $e(\alpha) = 2\exp(-\sigma^2 k_c^2) \cosh(\sigma^2 k_c^2 \cos \alpha)$ (cf.[14] for details). The coupling coefficients are given by $g_{jk} = (1 - \frac{1}{2}\delta_{jk})g(|\alpha_k - \alpha_j|)$ and $f_{jk} = (1 - \delta_{jk} - \delta_{jk-})f(|\alpha_k - \alpha_j|)$.
 - [24] The dynamics Eq. (7) has the real valued energy functional $E = \sum_j |A_j|^2 + \epsilon \sum_j (\bar{A}_j \bar{A}_j - e^{4i\frac{\pi}{n}j} + c.c.) - \frac{1}{2} \sum_{jk} g_{jk} |A_j|^2 |A_k|^2 - \frac{1}{2} \sum_{jk} f_{jk} A_k A_{k-} \bar{A}_j \bar{A}_{j-}$.